

See discussions, stats, and author profiles for this publication at: <http://www.researchgate.net/publication/283836615>

Precession-driven changes in Iceland–Scotland Overflow Water penetration and bottom water circulation on Gardar Drift since ~200ka

ARTICLE *in* PALAEOGEOGRAPHY PALAEOCLIMATOLOGY PALAEOECOLOGY · DECEMBER 2015

Impact Factor: 2.34 · DOI: 10.1016/j.palaeo.2015.09.042

READS

27

3 AUTHORS:



[Aurora Elmore](#)

Durham University

22 PUBLICATIONS 60 CITATIONS

[SEE PROFILE](#)



[James D Wright](#)

Rutgers, The State University of New Jersey

135 PUBLICATIONS 5,606 CITATIONS

[SEE PROFILE](#)

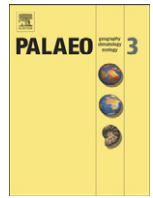


[Thomas Chalk](#)

Woods Hole Oceanographic Institution

2 PUBLICATIONS 8 CITATIONS

[SEE PROFILE](#)



Precession-driven changes in Iceland–Scotland Overflow Water penetration and bottom water circulation on Gardar Drift since ~200 ka



A.C. Elmore^{a,*}, J.D. Wright^b, T.B. Chalk^c

^a Department of Geography, Durham University, Durham DH1 3LE, England

^b Department of Earth and Planetary Sciences, Rutgers University, New Brunswick, NJ 08854, USA

^c Department of Physical Oceanography, Woods Hole Oceanographic Institution, 266 Woods Hole Road, Woods Hole, MA 02543, USA

ARTICLE INFO

Article history:

Received 16 March 2015

Received in revised form 21 September 2015

Accepted 23 September 2015

Available online 3 October 2015

Keywords:

North Atlantic Deep Water

Gardar Drift

Insolation

ABSTRACT

Benthic foraminiferal stable isotopic records from a transect of sediment cores south of the Iceland–Scotland Ridge reveal that the penetration depth of Iceland–Scotland Overflow Water (ISOW) varied on orbital timescales with precessional pacing over the past ~200 kyr. Similar, higher benthic foraminiferal $\delta^{13}\text{C}$ values (~1.0‰) were recorded at all transect sites downstream of the Iceland–Scotland Ridge during interglacial periods (Marine Isotope Chrons 5 and 1), indicating a deeply penetrating ISOW. During glacial periods (Marine Isotope Chrons 6, 4, and 2), benthic foraminiferal $\delta^{13}\text{C}$ values from the deeper (2700–3300 m), southern sites within this transect were significantly lower (~0.5‰) than values from the northern (shallower) portion of the transect (~1.0‰), reflecting a shoaling of ISOW and greater influence of glacial Southern Component Water (SCW) in the deep Northeast Atlantic. Particularly during intermediate climate states, ISOW strength is driven by precessional cycles, superimposed on the large-scale glacial–interglacial ISOW variability. Millennial-scale variability in the penetration of ISOW, likely caused by high-frequency Heinrich and Dansgaard–Oeschger events, is most pronounced during intermediate climate states.

© 2015 Elsevier B.V. All rights reserved.

1. Introduction

Variability in the formation of deep Northern Component Water (NCW; analogous to modern North Atlantic Deep Water; NADW) is linked to regional and global climate changes on orbital timescales (e.g., Broecker and Denton, 1989; Raymo et al., 1989). Causal mechanisms for variations in NCW formation are thought to be associated with incoming solar radiation (insolation), fresh-water input (Elmore and Wright, 2011; Elmore et al., 2015), and/or sea ice extent (Broecker and Denton, 1989; Rind et al., 2001; Dokken et al., 2013). During the late Pleistocene, changes in insolation in the high northern latitudes were the product of the combined influences of variations in the Earth's orbital parameters of eccentricity (~400 kyr and 100 kyr), obliquity (~40 kyr) cycles, and precession (~23 kyr) (Laskar et al., 1993). Since past variations in NCW production are tied to climatic conditions (including surface water temperature and wind strength), studies have linked particular NCW circulation patterns to different climate states, notably the glacial and interglacial end members (e.g., Broecker et al., 1985; Imbrie et al., 1993; Lisiecki et al., 2008). However, insolation

changes are not simply sinusoidal because the total insolation received is derived from distinct orbital periodicities (Laskar et al., 1993); and therefore, the deep-water circulation states may be unique for each glacial and interglacial period, as well as for intermediate climate states. Thus, there is significant scope for variations of NCW production to change both on glacial–interglacial timescales and with the precise orbitals associated; however, these NCW variations remain unresolved.

Modern NADW is produced by the interplay between five intermediate to deep water-mass components, Iceland–Scotland Overflow Water (ISOW; ~5 Sv), Denmark Strait Overflow Water (DSOW; ~5 Sv), Antarctic Bottom Water (AABW; ~1 Sv), Labrador Sea Water (~1 Sv), and Mediterranean Outflow Water (~1 Sv) (Worthington, 1976). Kuijpers et al. (1998) suggested that ISOW is the most important water mass for forming NADW; however, uncertainty remains as to the historical flux, strength, and penetration depth, related to the density of ISOW, particularly during intermediate climate states. While variability in each of the components of NADW is not fully understood, it has been proposed that changes in these components have contributed to the orbital-scale climate variability (Hillaire-Marcel et al., 1994; Raymo et al., 2004; Millo et al., 2006). Iceland–Scotland Overflow Water forms by convection in the Norwegian and Greenland Seas and the Arctic Ocean (Worthington, 1976; Mauritzen, 1996) and penetrates to >4 km depth (Dickson et al., 1990). The total contribution of ISOW is

* Corresponding author.

E-mail address: aurora.elmore@durham.ac.uk (A.C. Elmore).

related to surface temperature and salinity in the Nordic Seas (Duplessy et al., 1988a), as well as to the volume of surface inflow (Worthington, 1976), amount of sea ice cover (Prins et al., 2002; Raymo et al., 2004), wind forcing (Kohl et al., 2007), and regional tectonics (Wright and Miller, 1996). Sea-level and sill depth assert a control on ISOW contribution because they regulate the sensitive cross-sectional volume above the Iceland–Scotland–Faeroe Ridge, through which overflow water can pass between the open North Atlantic and the Nordic Seas (Millo et al., 2006). Thus, researchers suggested that ISOW strength and penetration depth have varied on timescales of millions of years (Wright and Miller, 1996), tens of thousands of years (i.e. orbital scale; Duplessy et al., 1988a; Raymo et al., 2004), thousands of years (i.e. millennial; Oppo et al., 1995; Dokken and Hald, 1996; McManus et al., 1999), hundreds of years (Bianchi and McCave, 1999; Moffa-Sanchez et al., 2015), years (Turrell et al., 1999), or seasons (Hátún et al., 2005).

Iceland–Scotland Overflow Water formation was likely vigorous and deeply penetrating during interglacial Marine Isotope Chron (MIC) 1 and 5e (Duplessy et al., 1988a,b; Kissel et al., 1997) and weaker and/or less deeply penetrating during the Last Glacial Maximum (LGM; MIC 2; Duplessy et al., 1988a; Kissel et al., 1997; Yu et al., 2008; Sarnthein et al., 2007); however, the history of ISOW is unclear for other glacial and intermediate climate states. For instance, Kuijpers et al. (1998) argued for enhanced formation of ISOW during MIC 6, while Kissel et al. (1997) and Rasmussen et al. (2013) considered it minimal. Kissel et al. (1997) presumed ISOW was vigorous during MIC 5d, while Kuijpers et al. (1998) and Rasmussen et al. (2013) suggest it was minimal. Additionally, several studies suggest that ISOW was vigorous during MIC 3 (Duplessy et al., 1988b; Kissel et al., 1997; Kuijpers et al., 1998), while others suggest a variable ISOW due to higher-frequency Heinrich Events and Dansgaard–Oeschger Cycles (Rasmussen et al., 1996a,b; Kissel et al., 1999; Prins et al., 2001, 2002; Rasmussen and Thomsen, 2009). Because ISOW is a large contributor to NCW (Schmitz and McCartney, 1993; Kissel et al., 1997; Hansen and Osterhus, 2000), variations in ISOW strength have been proposed to exert a large control over NCW circulation patterns (Kuijpers et al., 1998).

Large-scale deepwater circulation patterns in the North Atlantic have been reconstructed using geochemical records from benthic foraminiferal Cd/Ca (Boyle and Keigwin, 1987), Zn/Ca (Marchitto et al., 2002), ϵ_{Nd} (Yu et al., 2008; Roberts et al., 2010; Crocket et al., 2011), and especially $\delta^{13}\text{C}$ (e.g., Boyle and Keigwin, 1987; Oppo and Fairbanks, 1987; Duplessy et al., 1988a; Raymo et al., 1990; Sarnthein et al., 1994; Oppo and Lehman, 1995; Oppo et al., 1995; Flower et al., 2000; Curry and Oppo, 2005; Olsen and Ninnemann, 2010). Modern NADW is nutrient depleted, and thus, has high $\delta^{13}\text{C}$ values (1–1.5‰; Kroopnick et al., 1972; Kroopnick, 1985); modern NADW includes reintruded North Atlantic waters as well as contributions of ISOW, DSOW, and LSOW, which have $\delta^{13}\text{C}$ values of ~0.8‰, ~0.8‰ (Bauch et al., 2001; Dokken et al., 2013), and 0.8–1.2‰ (Winsor et al., 2012), respectively. In contrast, the nutrient-enriched Southern Ocean is vertically well mixed due to the strong West Wind Drift, and thus has an isotopic composition of $\delta^{13}\text{C}$ ~0.4‰ (Kroopnick, 1985). Deep Pacific Ocean $\delta^{13}\text{C}$ values are ~0.0‰, reflecting the long residence time of these waters (Kroopnick, 1985). As such, measured $\delta^{13}\text{C}$ values of biogenic calcite in the deep Southern Ocean reflect the relative inputs of deepwater masses from the Pacific, Indian, and Atlantic Oceans (Oppo

and Fairbanks, 1987; Charles and Fairbanks, 1992; Lynch-Stieglitz et al., 2007).

During glacial–interglacial transitions of the late Pleistocene, benthic foraminiferal $\delta^{13}\text{C}$ studies, supported by other geochemical studies, determined that the large-scale patterns of deepwater circulation vary between glacial and interglacial climate states (Boyle and Keigwin, 1987; Oppo and Fairbanks, 1987; Duplessy et al., 1988a; Oppo and Lehman, 1995; Roberts et al., 2010; Gebbie, 2014). Cross-sections of benthic foraminiferal $\delta^{13}\text{C}$ values of the Atlantic during the LGM (GEOSECS; Curry et al., 1988; Oppo and Horowitz, 2000; Venz and Hodell, 2002; Raymo et al., 2004; Curry and Oppo, 2005) show that a shoaling of NCW currents allowed for the northward intrusion of Antarctic Bottom Water (AABW) into the northern North Atlantic, up to 60°N. Studies have therefore suggested that the core of NCW shoaled by as much as ~2 km during the LGM (Curry et al., 1988; Duplessy et al., 1988a; Sarnthein et al., 1994; Oppo and Lehman, 1995; Gebbie, 2014), coincident with a weakened and/or shallower ISOW (Duplessy et al., 1988b; Kissel et al., 1997; Yu et al., 2008).

The objective of this study was to determine variability in deepwater circulation patterns in the eastern North Atlantic over the past 200 kyr on orbital and millennial timescales. Herein, new $\delta^{13}\text{C}$ records from sediment cores 11JPC and 3GGC, from the southern end of Gardar Drift, are presented for the past 200 ka (Fig. 1A). New records from these two cores are combined with published records from seven other cores with a variety of depths and sufficient data within the interval of interest to form our “Gardar Drift Transect” (Table 1; Fig. 1). This transect provides a unique opportunity to track variations in the influence of ISOW. Transect cores, combined with cores from the South Atlantic (Ocean Drilling Program; ODP Site 1090) and mid-latitude North Atlantic (Deep Sea Drilling Program; DSDP Site 607), allow for the examination of southern sourced waters in the eastern northern North Atlantic in a similar method to the Atlantic cross-sections (e.g., Curry and Oppo, 2005), but on a finer scale (Fig. 1B). To examine the depth to which ISOW penetrated, benthic foraminiferal $\delta^{13}\text{C}$, a semi-conservative water mass tracer, was compared along a depth transect south of the Iceland–Scotland Ridge, with the occurrence of low $\delta^{13}\text{C}$ water on southern Gardar Drift (here taken to be southern sourced) being indicative of a shoaled ISOW.

2. Methods

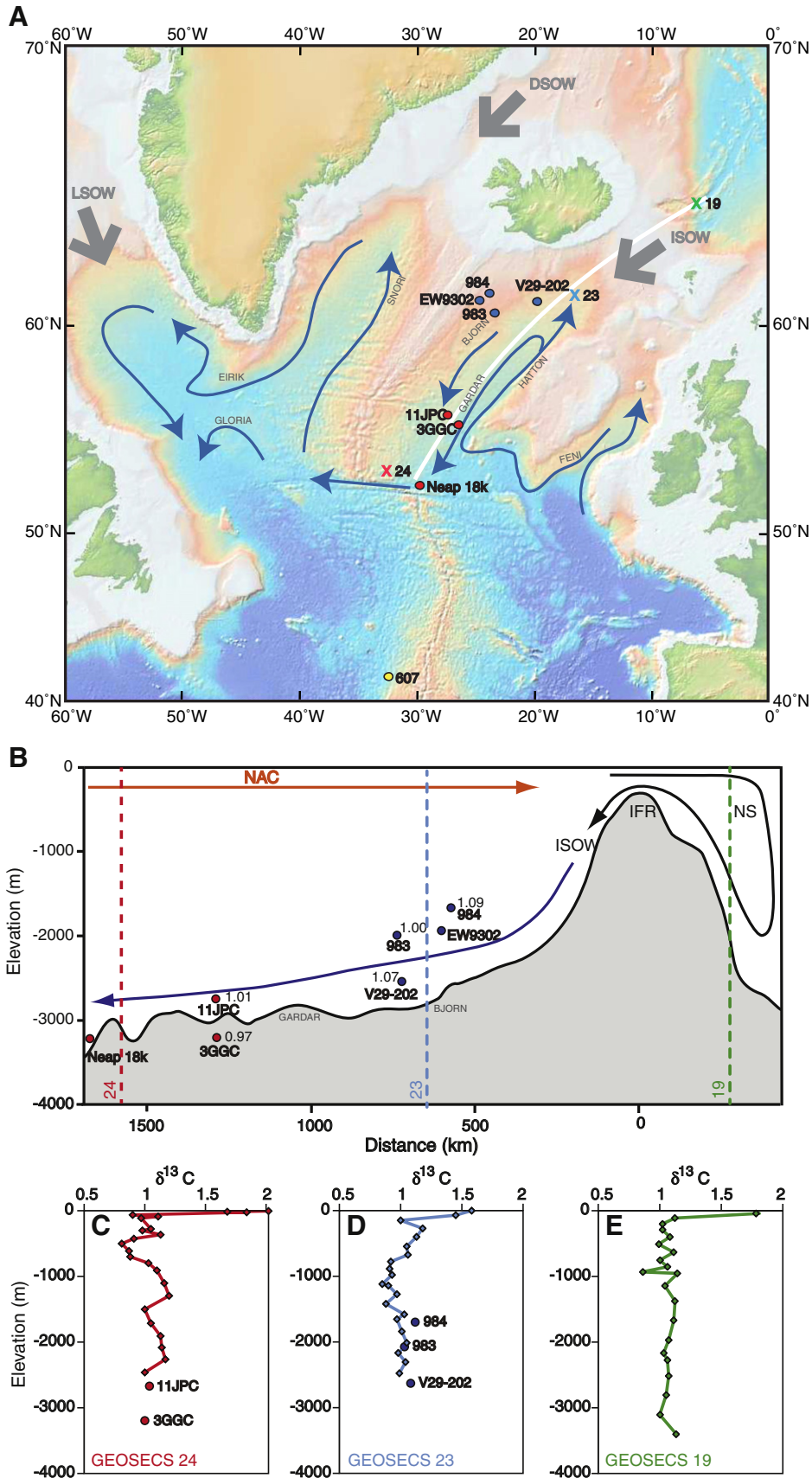
2.1. Regional setting

Gardar and Bjorn Drifts are key deposits for studying North Atlantic paleoceanography since they lie within the flow of modern-day ISOW (Fig. 1A; e.g., Oppo and Lehman, 1995; Bianchi and McCave, 1999). As ISOW flows south along the Reykjanes Ridge, contourite drift deposits form along each edge of the current, with Bjorn Drift to the north and Gardar Drift to the South (Fig. 1A; Davies and Laughton, 1972; Bianchi and McCave, 1999). Contourite drifts, like Gardar and Bjorn, are found throughout the North Atlantic where large quantities of sediments are ‘plastered’ against already existing bathymetric features (Hollister et al., 1978). These contourite drift deposits provide an excellent location for paleoceanographic reconstructions due to the high sedimentation rates (Fig. 1A; e.g., McCave et al., 1980; McCave and Tucholke, 1986; Channell et al., 1997; Hall et al., 1998; Bianchi and McCave,

Fig. 1. A. Bathymetric map of the North Atlantic, including bottom water currents (blue), contourite drifts (uppercase lettering), and the northern components of NADW; ISOW, DSOW, and LSOW (grey arrows). Core locations from this study and previously published studies are shown, including northern Gardar Drift sites (blue); ODP 984, EW9302, V29-202, and ODP983, and southern Gardar Drift sites (red); 11JPC (this study), 3GGC (this study), and Neap 18k. The location of the cross-section in Fig. 1B is designated by the white line. GEOSECS stations for the $\delta^{13}\text{C}$ data presented in Figs. 1C, D, and E are designated by a cross for station 24 (red), 23 (blue), and 19 (green). B. Bathymetric cross-section of the southern Norwegian Sea (NS) and the region south of the Iceland–Faeroes Ridge (IFR), as shown by the white line on Fig. 1A. Bold lines show idealized directions of the major modern water masses, North Atlantic Current (NAC; orange), and Iceland–Scotland Overflow Water (ISOW; navy). The location of Bjorn and Gardar Drifts are shown, as are the projected locations of all cores used in this study (blue circles for northern Gardar Drift and red circles for southern Gardar Drift). Late Holocene *P. wuellerstorfi* $\delta^{13}\text{C}$ values from the selected cores are shown, where available. The vertical dashed lines represent the locations of recently measured profiles from GEOSECS stations 24 (red; C), 23 (blue; D), and 19 (green; E; Kroopnick et al., 1972). Coretop benthic foraminiferal $\delta^{13}\text{C}$ data from cores used in this study are included where available.

1999; Faugers et al., 1999; Praetorius et al., 2008; Thornalley et al., 2010, 2011a; Elmore and Wright, 2011; Elmore et al., 2015). To utilize the paleoceanographic information in this archive, the study examined

jumbo piston core, 11JPC (2707 m), and giant gravity core, 3GGC (3305 m; Table 1; Fig. 1). Both cores were collected by the R/V Knorr from southern Gardar Drift on cruise 166, leg 14 in 2002.



2.2. Samples and sedimentological data collection

To generate estimates of weight percent of carbonate (Wt. % CaCO₃) and weight percent of coarse fraction (Wt. % CF), we sampled cores 11JPC and 3GGC at ~5 cm intervals for the entire length of both cores (23.60 m for 11JPC and 1.84 m for 3GGC). Samples were split approximately in half and each half was dried overnight in a 50 °C oven. One half of each sample was weighed (Dry Wt._{initial}) and combined with ~40 ml of 1.0 M acetic acid in a 50 ml centrifuge tube for 24 hours. Each sample was agitated during the process to ensure complete removal of carbonate from the sample. The vials were centrifuged for 1 minute to separate the sample from the acid, which was then decanted. Samples were reprocessed in acetic acid and then rinsed with 40 ml of deionized water three times, centrifuging for 1 minute before each decanting. Samples were then oven-dried and weighed again (Dry Wt._{CaCO₃}). Assuming negligible opal content since biogenic silica was not observed during microscopic examination, the weight percent calcium carbonate (Wt. % CaCO₃) was then determined using the following equation:

$$\text{Wt. \% CaCO}_3 = (1 - \text{Dry Wt.}_{\text{CaCO}_3} / \text{Dry Wt.}_{\text{initial}}) * 100 \quad (1)$$

Weight percent coarse fraction (Wt. % CF) was determined by weighing the other half of the dried sample before (wt._{unwashed}) and after (wt._{washed}) being washed through a 63 µm sieve. Dry samples were soaked in a dilute calgon solution to prevent flocculation during washing. Wt. % CF was then calculated using the following equation:

$$\text{Wt. \% CF} = (\text{wt.}_{\text{washed}} / \text{wt.}_{\text{unwashed}}) * 100 \quad (2)$$

2.3. Stable isotopic analysis

In order to assess the paleoceanographic changes over Gardar Drift since 200 ka, stable isotopic analyses of δ¹⁸O were performed on benthic foraminifera to establish age control (e.g., Lisiecki and Raymo, 2005), and the simultaneous analysis of δ¹³C was measured since epifaunal benthic foraminifera faithfully record changes in the δ¹³C value of the bottom waters in which they live (e.g., Curry and Oppo, 2005). For this study, only *P. wuellerstorfi* tests were chosen for benthic foraminiferal analysis since some *Cibicides* taxa (e.g., *C. robertsoniensis*) do not record equilibrium values and may be up to 1‰ lower in δ¹³C values in this region (Elmore, 2009). Planktic foraminifera were also analyzed for stable isotopic concentration to ensure that changes in surface productivity were not a controlling factor on benthic δ¹³C values (Mackensen et al., 1993).

For stable isotopic analyses, ~15 tests of the planktic foraminifera, *Globigerina bulloides*, and ~5 tests of benthic foraminifera, *Planulina wuellerstorfi*, were handpicked under a binocular microscope from the 250–350 µm size fraction of the washed samples. The samples were analyzed using a Micromass Optima Mass Spectrometer equipped with an automated Multiprep at the Rutgers University Stable Isotope Laboratory. Samples were reacted in phosphoric acid for 15 minutes at 90 °C. Measured values are reported using standard δ-notation and are compared to Vienna PeeDee Belemnite using an internal lab standard that is routinely calibrated with NBS-19 (1.95‰ δ¹³C, –2.20‰ δ¹⁸O; Coplen et al., 1983). The internal lab standard is offset from NBS-19 by 0.1‰ for δ¹³C and 0.04‰ for δ¹⁸O. The 1-σ precision of standards during analysis for this project was typically 0.05‰ for δ¹³C and 0.09 ‰ for δ¹⁸O.

Differences between bottom water δ¹³C values are the result of the waters' source region (δ¹³C values are biologically fractionated during primary productivity and undergo temperature-dependent fractionation during air-sea gas exchange; Lynch-Stieglitz et al., 1995); δ¹³C values are also controlled by water mass ageing and productivity fluctuations above the waters' flow path. Additionally, benthic foraminiferal δ¹³C values can be affected by organic carbon settling to the deep sea above the site, which is controlled by primary productivity and remineralization (Mackensen et al., 1993). Thus, benthic foraminiferal δ¹³C records at a particular site may also contain a localized signal relating to changing organic carbon flux and/or water mass remineralization properties. For southern Gardar Drift Sites for which data are presented here, there are no significant similarities between the planktic and benthic δ¹³C records within each core (Figs. 2, 3), indicating that surface processes are not dominating the benthic foraminiferal δ¹³C signal. Similar δ¹³C values among all Gardar Drift sites (Fig. 5C), especially during interglacials, provide additional confidence in the use of δ¹³C as a reliable water mass tracer on Gardar Drift (Praetorius et al., 2008; Thornalley et al., 2010, 2011a; Elmore and Wright, 2011; Elmore et al., 2015). Thus, for the remainder of this manuscript, our Gardar Drift benthic foraminiferal δ¹³C data have been confidently used as a paleo-watermass tracer.

2.4. Age models

The age model for the top 333 cm of 11JPC was constrained by 15 AMS ¹⁴C ages (Table 2), which were all previously published in Elmore and Wright (2011) and Elmore et al. (2015). As previously published, the AMS samples were composed of 4–6 mg of planktic foraminifera *Globigerina bulloides* that were selected using a binocular microscope, ultra sonicated in deionized water, and analyzed at the Keck Center for Accelerator Mass Spectrometry at the University of California, Irvine (Elmore and Wright, 2011). These published

Table 1
Locations and water depths of cores used in this study.

Core	Lat	Lon	Water depth (m)	Age model reference	Interval in compilation	Average age resolution (kyr per sample)
<i>Northern Gardar Drift sites:</i>						
ODP site 984	61.43	–24.08	1660	Raymo et al. (2004)	0–210 ka	1.30
EW9302 JPC8	61.00	–25.00	1915	Oppo et al. (2001); Oppo et al. (1997)	57–135 ka	0.54
ODP site 983	60.40	–23.63	1995	Jansen et al. (1996); McIntyre et al. (1999); Raymo et al. (1998); Kleiven et al. (2003); Raymo et al. (2004);	0–210 ka	0.81
V29-202	61.00	–21.00	2658	Oppo and Lehman (1995)	0–160 ka	0.62
<i>Southern Gardar Drift sites:</i>						
KN166-14 11JPC	56.24	–27.65	2707	This study	0–13 ka & 33–210 ka	0.92
KN166-14 3GGC	55.52	–26.53	3305	This study	0–27 ka	0.40
Neap 18k	52.77	–30.35	3275	Chapman and Shackleton (1999)	55–125 ka	0.65
<i>Atlantic sites (not included in the compilation):</i>						
DSDP site 607	41.00	–32.96	3427	Raymo et al. (2004)		
ODP site 1090	42.91	–8.90	3702	Venz and Hodell (2002)		

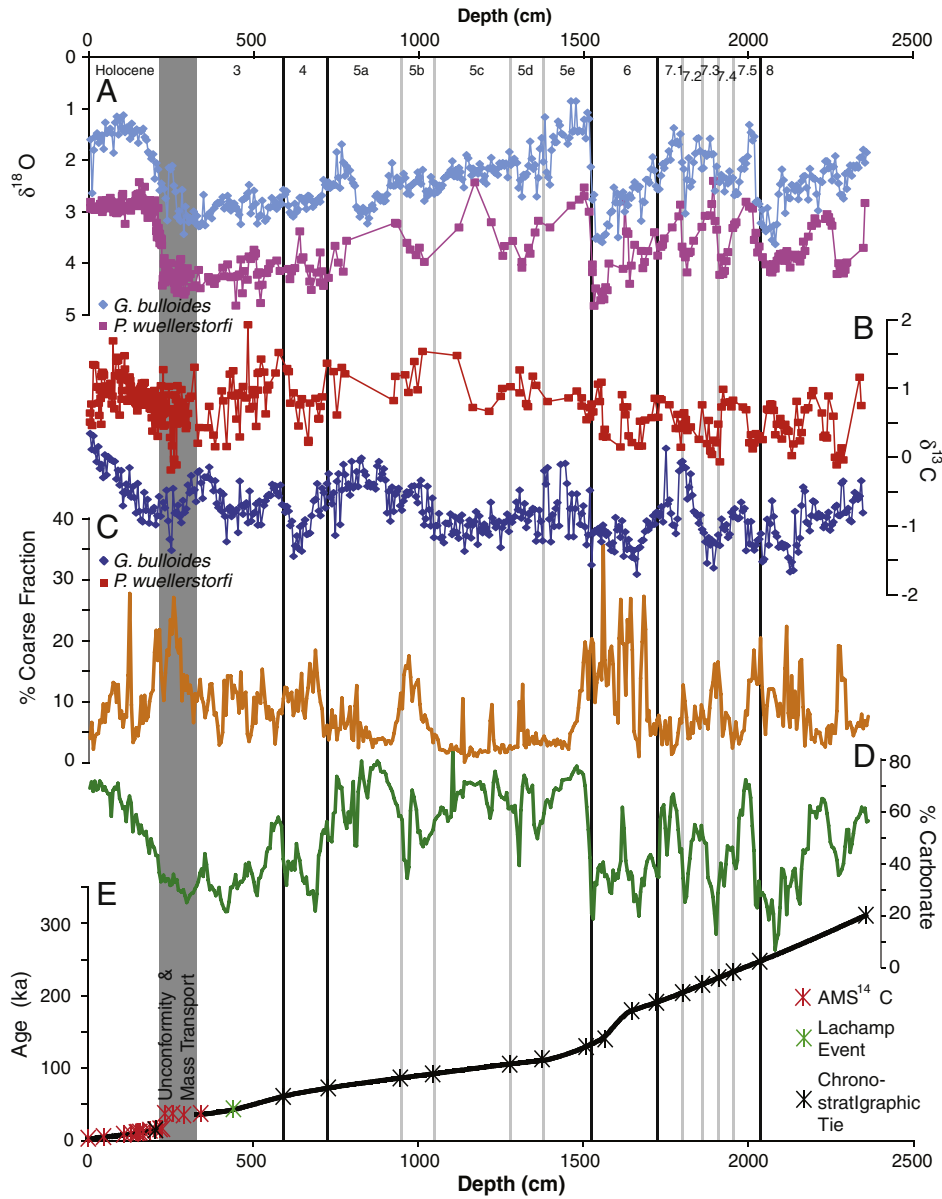


Fig. 2. Proxy records from core 11JPC plotted versus sediment depth. (A) $\delta^{18}\text{O}$ *G. bulloides* (light blue) and $\delta^{18}\text{O}$ *P. wuellerstorfi* (red), (B) $\delta^{13}\text{C}$ *G. bulloides* (blue) and $\delta^{13}\text{C}$ *P. wuellerstorfi* (red), (C) % CF (orange), (D) % CaCO_3 (green), and (E) the age model with age-depth tie points are shown. Marine Isotope Chrons 1 through 8 are also shown.

radiocarbon ages were then converted to calendar ages according to the Fairbanks0805 calibration, and a standard 400-year reservoir correction was applied (Fairbanks et al., 2005). Since the publication of these AMS ^{14}C dates, temporally evolving reservoir age corrections have been proposed for studies of cores from this region (Thornalley et al., 2011b; Stern and Lisiecki, 2013), application of constant correction/adjustment does not change the conclusions of this study because 1) the majority of our study interval (210–40 ka) is earlier than the utility of AMS ^{14}C dating (40 ka to present), and 2) the standard reservoir correction was also consistently applied to any AMS ^{14}C dates used in the previously published age models. We are not endeavoring to look at the high-frequency variations among these cores and thus any relatively minor offsets in age models will not significantly affect the conclusions in this study. The published age model from Elmore and Wright (2011) revealed a ~18 kyr hiatus, constrained by 3 AMS ^{14}C dates from 227 to 282 cm (Table 2). Based on an abrupt color change in the core, the top of this hiatus was located at 222 cm (see supplement of Elmore and Wright,

2011). This section of sediment is interpreted to represent a mass transport event and thus data from this interval were not interpreted as part of this study. The previously published AMS ^{14}C date of ~33.81 ka at 333 cm is considered to be below the mass transport event because it conforms to the linear sedimentation rate defined by the remainder of chrono-stratigraphic tie points below the event (Fig. 2E).

Age model information below 333 cm is not based on radiocarbon and is being presented here for the first time. The Lachamp Event (40 ka) was identified at 430 cm (H. Evans, personal communication; Table 2). Additional chrono-stratigraphic tie points were determined by comparing measured foraminiferal $\delta^{18}\text{O}$ values to a stacked, benthic foraminiferal $\delta^{18}\text{O}$ record by Lisiecki and Raymo (2005) (Table 2). The error associated with the Lisiecki and Raymo (2005) stack is reported to be ~2 kyr, though relative errors will be significantly lower at individual sites tied to the LR04 chronology. In the case of 11JPC, the benthic foraminiferal $\delta^{18}\text{O}$ *P. wuellerstorfi* record shows a very strong agreement to the LR04 stack as well as to the other records in the region (Fig. 4) and the

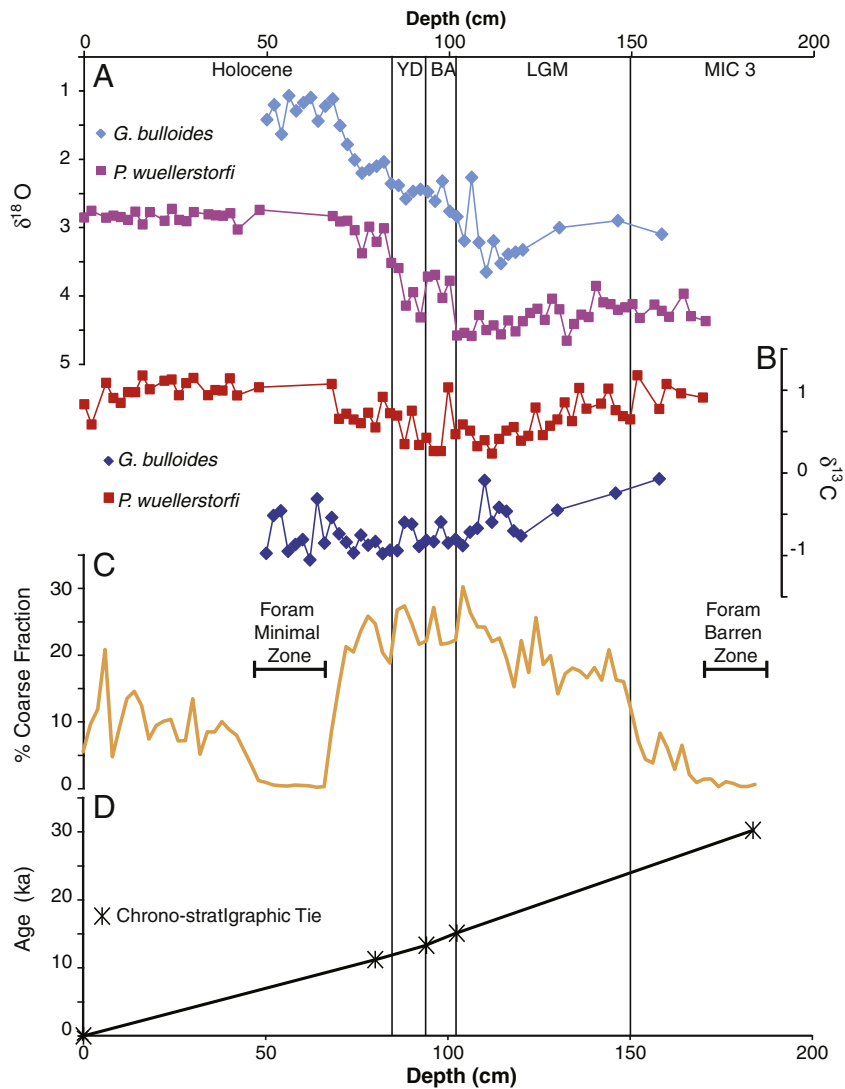


Fig. 3. Proxy records for core 3GGC plotted versus sediment depth. (A) $\delta^{18}\text{O}$ *G. bulloides* (light blue) and $\delta^{18}\text{O}$ *P. wuellerstorfi* (pink), (B) $\delta^{13}\text{C}$ *G. bulloides* (blue), and $\delta^{13}\text{C}$ *P. wuellerstorfi* (red), (C) % CF (orange), (D) the age model, with age–depth tie points is shown. The Holocene, Younger Dryas (YD), Bolling/Allerod (BA), Last Glacial Maximum (LGM) and MIC 3 are also indicated.

age model shows nearly linear sedimentation rates through the interval of study (Fig. 2E).

An age model for 3GGC was established based entirely on visual correlation among similar records (i.e., wiggle matching) rather than AMS ^{14}C dating (see Table 3), thus cores 3GGC and 11JPC are on a common age model. The record of benthic $\delta^{18}\text{O}$ from 3GGC (Fig. 3A) was first visually compared to the Lisiecki and Raymo (2005) LR04 stack. A further, fine-tuning of the age model was completed by visual comparison of benthic and planktic $\delta^{18}\text{O}$, benthic $\delta^{13}\text{C}$, % CF, and % CaCO_3 from GGC 3 to the proximal core, 11JPC (Fig. 3; Table 3). Since there are no available AMS ^{14}C dates, the error associated with this age model is proportionate to the error reported for the LR04 benthic stack of ~2 kyr.

As with the previously published age model from Elmore et al. (2015) and Elmore and Wright (2011) that constrains the ages for the top of 11JPC, all previously published benthic foraminiferal $\delta^{13}\text{C}$ records used in the construction of the Gardar Transect were kept on their originally published chronologies (Table 1). The selected cores each have substantial resolution to be used for comparison, with each published measured sample representing between 0.4 and 1.3 kyr of sedimentation (Table 1). Thus, these cores are ideally geographically located and capable of comprising a depth transect to trace watermass changes on Gardar Drift (Fig. 1). To support the use of each chronology remaining

as it was published, there is a remarkable similarity in trends and values of the $\delta^{18}\text{O}$ records from all sites investigated here, when the original benthic foraminiferal $\delta^{18}\text{O}$ data are compared (Fig. 4). Since benthic foraminiferal $\delta^{18}\text{O}$ is largely controlled by extra-regional processes (including continental ice volume), the similarity in records is a strong indication that the age models for these sites are comparable, and relatively minor offsets will not affect the conclusions of this study.

2.5. Transect construction

To evaluate ISOW changes in the Late Pleistocene, we compiled the benthic foraminiferal $\delta^{13}\text{C}$ data from all available core locations with high-resolution data over the time period of interest (Table 1). The range in length (1600 km), range in water depth (1600 m), and confined geographic area of the sites within the Gardar Drift transect allows for the detection of ISOW penetration depth by monitoring variations in benthic foraminiferal $\delta^{13}\text{C}$ values (Fig. 1). Fig. 5C shows our new $\delta^{13}\text{C}_{P. wuellerstorfi}$ data, as well as all previously published (i.e., raw) data from the cores used to form the Gardar transect, on their original age models. To assess this variability in $\delta^{13}\text{C}$ gradients on Gardar Drift, data from each of the sites in the Gardar transect were treated in two ways. First, benthic foraminiferal $\delta^{13}\text{C}$ data from all sites in the Gardar

Table 2

Age model for core KN166-14 11JPC was previously published for 0 to 33.81 ka (Elmore and Wright, 2011) and the interval from 33.81 to the bottom of the core is presented here for the first time. Tie points were determined by AMS ^{14}C (white boxes), magneto-stratigraphy (orange box), or chrono-stratigraphic comparison to a stacked benthic foraminiferal $\delta^{18}\text{O}$ record by Lisiecki and Raymo (2005); (blue boxes). AMS ^{14}C ages in red were not included in the age model (Elmore and Wright, 2011).

Depth (cm)	Age (ka)
0	0.67
45	2.87
105	6.05
127	7.06
143	8.38
145	6.99
147	8.58
149	8.86
153	8.88
163	9.65
183	11.45
198	11.99
213	13.34
220	13.62
227	34.07
250	33.71
282	31.91
333	33.81
430	40.00
626	62.70
779.7	74.50
1003	88.00
1260	103.00
1394	110.00
1518	129.30
1558	138.20
1636	174.50
1795	201.00
1929	226.00
2083	254.00
2290	295.00

region from 0 to 200 ka (Fig. 5C) were smoothed using a Gaussian fit with a span of 2 kyr. This provided an average benthic foraminiferal $\delta^{13}\text{C}$ value. Uncertainties for this average were calculated by using a Monte Carlo simulation, where the external reproducibility of the data was taken into account. This was performed by perturbing the $\delta^{13}\text{C}$ data over a large sample number ($n = 1000$), and summing the resultant records before smoothing (as above) over a 2-kyr window. All sites were weighted equally (where they contained data within the sampling window, i.e., gaps of >2 kyr are omitted) to provide an unbiased final compilation. The standard deviation from the mean was then calculated along the timeseries (Fig. 5E).

Secondly, Gardar Drift core sites were divided into North and South regions (Fig. 1) to examine watermass changes along the drift crest. For the Northern Gardar Transect, a composite record was generated for northern sites, ODP site 984, ODP site 983, EW9302 JPC8, and V29-202. The weighted mean for Northern Gardar and 95% confidence intervals are presented along with the standard deviations from the mean, calculated as above (Fig. 5F). A composite record for the sites on Southern Gardar, 11JPC, 3GGC, and Neap 18k, was determined

using the same method (Fig. 1). The difference between the North Gardar transect benthic foraminiferal $\delta^{13}\text{C}$ record and the South Gardar transect $\delta^{13}\text{C}$ records was then determined, utilizing the full uncertainty characterized by the composites (Fig. 5G). All Monte Carlo statistics were carried out in the R statistical analysis program (R Development Core Team, 2010).

Timeseries analyses were completed on the north–south difference and standard deviation of the benthic foraminiferal $\delta^{13}\text{C}$ transect data using the AnalySeries 2.0.4.2 program (Paillard et al., 1996) using a span of 0.01 to identify recurring periodicities (Fig. 6). Spectral analyses were completed using the –Tukey method in the same software (Blackman and Tukey, 1958).

The $\delta^{13}\text{C}$ value of the Southern Component Water (SCW) end member was determined by using ODP Site 1090 from the Atlantic sector of the Southern Ocean (Table 1). As an additional monitor of the intrusion of SCW into the North Atlantic, benthic foraminiferal $\delta^{13}\text{C}$ data were included from ODP Site 607, located below the subtropical North Atlantic (Raymo et al., 1989; Ruddiman et al., 1989). Core locations, water depths, and age model information for each site are provided in Table 1.

3. Results

3.1. Core KN166-14 11JPC

Marine Isotope Chronozones (MIC) 1 through 9a were defined in core 11JPC using the planktic and benthic oxygen isotope records, which show the typical saw-toothed pattern that characterized the late Pleistocene benthic foraminiferal oxygen isotope curves (Lisiecki and Raymo, 2005; Fig. 4). Over this interval, the $\delta^{18}\text{O}$ values range from 0.8 to 3.8‰ for *G. bulloides*, and from 2.5 to 4.5‰ for *P. wuellerstorfi* (Fig. 2). Sharp decreases in $\delta^{18}\text{O}$ are recorded at transitions from glacial to interglacial chronozones (MIC 8–7.5, MIC 6–5e; Fig. 2).

Benthic foraminiferal $\delta^{13}\text{C}$ records from core 11JPC record orbital-scale variability, with values from -0.3 to 1.5% for *P. wuellerstorfi* (Fig. 2). The lowest values in benthic $\delta^{13}\text{C}$ are recorded during MIC 8, 6, 4, and 3 (Fig. 2). Values of benthic $\delta^{13}\text{C}$ are highly variable during MIC 3, likely due to the high-frequency Heinrich or Dansgaard–Oeschger Events (Fig. 2).

Through the interval of study, the record of Wt. % CF varies on glacial–interglacial timescales with values ranging from 0 to 35% for core 11JPC (Fig. 2). Low Wt. % CF (<15%) values are recorded during interglacial MICs 7.5, 7.3–7.1, 5e–5c, 5a, and 1 (Fig. 2). The highest Wt. % CF values are recorded from 1700 to 1550 cm, corresponding to MIC 6 (Fig. 2). The observed variability in Wt. % CF values indicate either an increase in fine particles during interglacials, an increase of large particles during glacials, or both (Fig. 2); winnowing or dissolution could also affect the Wt. % CF record; however, foraminifera appear visually well preserved. Increased ice rafted detritus (IRD) abundances during glacial periods are a well-documented feature of North Atlantic sediment records (Ruddiman, 1977; Bond and Lotti, 1995; McManus et al., 1999; Venz et al., 1999; Andrews, 2000) and have been documented during the cold Younger Dryas from this sediment core (Elmore and Wright, 2011); this suggests that higher glacial Wt. % CF is mainly due to a glacial increase in IRD (Fig. 2). The MIC 3 section is characterized by Wt. % CF values that are highly variable and range from 0 to 25%; this is likely caused by increased IRD during Heinrich Events (Bond and Lotti, 1995; Fig. 2).

Weight percent carbonate also varies on glacial–interglacial timescales in core 11JPC (Fig. 2), as has been shown in other North Atlantic cores (Ruddiman et al., 1987; Ortiz et al., 1999). Low Wt. % CaCO_3 values (20–30%) are recorded in the sections from 2200 to 2100, 1900 to 1800, 1600 to 1500, and 500 to 300 cm (Fig. 2). These low % CaCO_3 values are coincident with elevated % CF suggesting that the record of % CaCO_3 is determined mainly by the dilution of carbonate by larger IRD during glacial periods (Fig. 2). Highest values of % CaCO_3 are recorded in

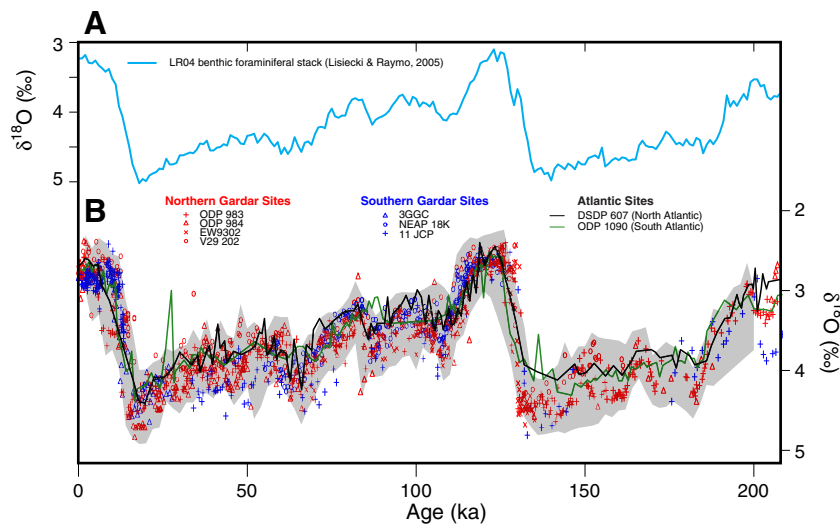


Fig. 4. A: The LR04 benthic foraminiferal stack (light blue; Lisiecki and Raymo, 2005) is shown for reference over our interval of interest. B: All benthic foraminiferal $\delta^{18}\text{O}$ data from northern portion of the Gardar Drift transect (red), the southern portion of the transect (blue), including our 2 new cores (11JPC and 3GGC). The very good correspondence between all records shows strong confidence in the age models of all cores. The 95% confidence interval of all data is shown in grey, which includes uncertainty propagated by a Monte Carlo ($n = 1000$) simulation.

11JPC sediments from 2100 to 2050, 1500 to 1450, 1275 to 1225, 950 to 800, and 150 to 0 cm (Fig. 2). These zones of high % CaCO_3 correspond to interglacial periods with high productivity (Fig. 2).

3.2. Core KN166-14 3GGC

According to the age model described above, core 3GGC can be subdivided into chronozones of the upper MIC 3, Last Glacial Maximum (LGM), Bolling/Allerod, Younger Dryas, and Holocene (Fig. 3). Oxygen isotope values for *G. bulloides* and *P. wuellerstorfi* are highest (~ 3.5 and 4.5% , respectively) in the LGM section (~ 25 – 15 ka; Fig. 3). Termination 1 is recorded by a decrease in the $\delta^{18}\text{O}$ values in all species, marking the Bolling/Allerod section. Increasing $\delta^{18}\text{O}$ values reflect the cooler conditions during the Younger Dryas section (~ 13.1 – 11.5 ka; Fig. 3). The lowest $\delta^{18}\text{O}$ values in 3GGC represent the Holocene section (~ 11.5 – 0 ka; Fig. 3).

Benthic and planktic $\delta^{13}\text{C}$ values decrease in the upper MIC3 and LGM sections for *G. bulloides* and *P. wuellerstorfi* (from 0.0 to -1.0 and from 1.2 to 0.4% , respectively); values of each species are similar in these sections (Fig. 3). *P. wuellerstorfi* $\delta^{13}\text{C}$ values increase in the Bolling/Allerod, Younger Dryas, and lower Holocene to values of 1.0 and 0.5% , respectively (Fig. 3). Unlike *P. wuellerstorfi*, *G. bulloides* $\delta^{13}\text{C}$ values decrease in the Bolling/Allerod, Younger Dryas, and lower Holocene to a value of -1.0 (Fig. 3).

The record of Wt. % CF is variable for core 3GGC, with values ranging from 0 to 35% (Fig. 3). Low Wt. % CF ($<10\%$) is observed in the upper MIC 3 and throughout MIC 1 (Fig. 3). Higher Wt. % CF ($>20\%$) is observed during the LGM, likely due to an increase in IRD (Fig. 3; McManus et al., 1999).

Table 3

Age model for core KN166-14 3GGC was determined based on chrono-stratigraphic comparison to a stacked benthic foraminiferal $\delta^{18}\text{O}$ record by Lisiecki and Raymo (2005).

Depth (cm)	Age (ka)
0	0
82	11.5
94	13.3
102	15
184	30

3.3. Transect results

A comparison of benthic foraminiferal $\delta^{13}\text{C}$ records from sites down-stream of the Iceland–Scotland Ridge reveals a large degree of variability, indicating changes in watermasses (Fig. 5C). The sites in the southern portion of the transect show greater variability than those in the northern part (Fig. 5C; F). This is reflective of the greater influence of SCW, with low $\delta^{13}\text{C}$ values, recorded from sites that are more distal from the Iceland–Scotland Ridge (Fig. 5D). Lower variability in $\delta^{13}\text{C}$ values in the northern sites, or sites proximal to the ridge, indicates that they were almost always bathed by the same watermass with unchanging composition, which is likely ISOW (Fig. 5C). The difference in benthic foraminiferal $\delta^{13}\text{C}$ values between all transect sites is minimal ($<0.5\%$) during interglacials, MIC 5, and the Holocene, indicating that all transect sites were bathed by a similar water mass during interglacial periods (Fig. 5C, D). The benthic foraminiferal $\delta^{13}\text{C}$ values of the northern transect compilation and southern transect compilation are also similar during interglacial periods, also indicating that all of the transect sites were bathed by a similar watermass, likely ISOW (Fig. 5F).

The standard deviation from the ensemble mean of all benthic foraminiferal $\delta^{13}\text{C}$ data is less than 0.25% during interglacial periods (therefore within analytical reproducibility), providing statistical representations of the small gradient in benthic foraminiferal $\delta^{13}\text{C}$ values within the transect sites (Fig. 5E). The difference between the northern and southern transect composite benthic foraminiferal $\delta^{13}\text{C}$ records is also lower during interglacials ($<0.2\%$), indicating a small gradient in benthic foraminiferal $\delta^{13}\text{C}$ (Fig. 5F, G). The small increase in standard deviation values in the earliest portion MIC 5e is likely due to differences within the age models for individual records over the abrupt transition from MIC 6 to 5e (Fig. 5E). Since the northernmost cores used in this comparison (ODP site 984 and ODP site 983) lie northward of the maximum possible extent of AABW (Curry and Oppo, 2005), they should always record the $\delta^{13}\text{C}$ signature of a northern source and can be approximated as the northern end member (Raymo et al., 1989). The low variability in the benthic foraminiferal $\delta^{13}\text{C}$ records during the interglacial periods thus indicates that all sites are recording a northern sourced watermass during interglacial periods (Fig. 5E). Additionally, while benthic foraminiferal $\delta^{13}\text{C}$ values at DSDP site 607 are very similar to southern Gardar values during interglacial periods, benthic foraminiferal $\delta^{13}\text{C}$ values from the South Atlantic site (ODP site 1090) are significantly lower, suggesting that southern sourced waters were not

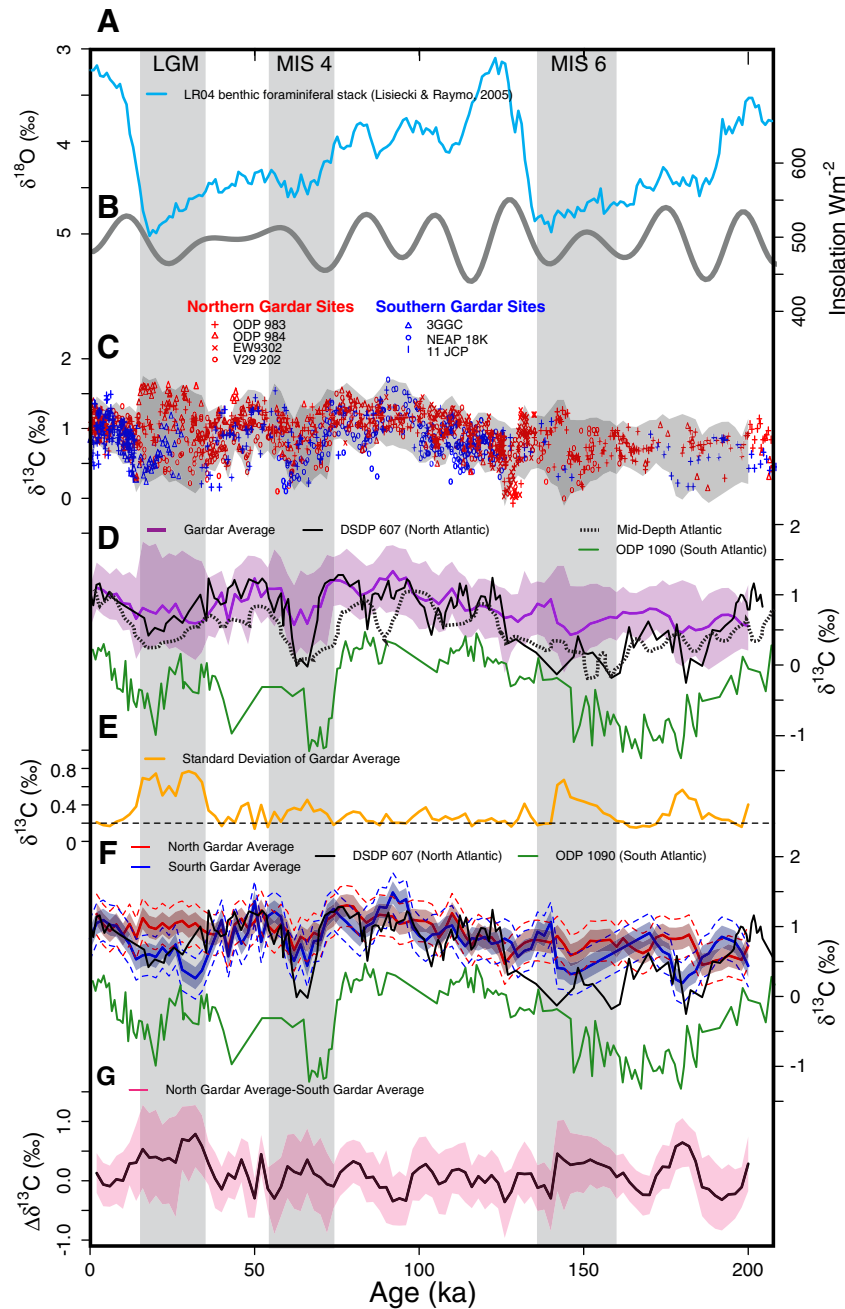


Fig. 5. A: The LR04 benthic foraminiferal stack (light blue; Lisiecki and Raymo, 2005) is shown for reference over our interval of interest. Light grey vertical bars indicate glacial intervals of LGM, MIS4, and MIS6. B: Insolation at 65°N for the last 200 kyr (grey; Laskar et al. 2004). C: All benthic foraminiferal $\delta^{13}\text{C}$ data from the northern portion of the Gardar transect (red symbols; ODP Site 984, EW9302 JPC8, ODP Site 983, and V29–202) and the southern portion of the transect (blue symbols; 11JPC, 3GGC, and NEAP18k) are shown with age, including the 95% confidence interval of all Gardar Drift data (grey swath). D: Average of all Gardar *P. wuellerstorfi* $\delta^{13}\text{C}$ values interpolated in 2-kyr intervals (black line) plotted with ± 2 standard deviation (purple swath) is shown versus age from 0 to 200 ka. The mid-latitude North Atlantic DSDP site 607 (black line) and South Atlantic ODP site 1090 (green line) are shown for comparison. The mid-depth Atlantic composite record from sites ODP925, ODP927, ODP928, and GeoB1214 from Lisiecki et al. (2008) is also shown (dashed line). E: Standard deviation of all Gardar transect $\delta^{13}\text{C}$ values interpolated in 2-kyr intervals (orange). F: The average of $\delta^{13}\text{C}$ *P. wuellerstorfi* records from the northern transect sites (red line), compared with the southern transect sites (blue line), both shown with associated confidence intervals (swaths). The mid-latitude North Atlantic (DSDP site 607; black line) and South Atlantic (ODP site 1090; green line) are again shown for comparison. G: The difference between $\delta^{13}\text{C}$ values of the smoothed northern and southern transects from panel F (black line with pink swath indicating the confidence intervals). Note: the northern quartet of sites and southern trio are given equal weighting.

prevalent in the northern North Atlantic during these periods (Fig. 5F). Thus, a small benthic foraminiferal $\delta^{13}\text{C}$ gradient during MIC 5e and the Holocene indicates that a deeply penetrating ISOW bathed all sites on Gardar Drift (Fig. 5G).

The gradient in benthic foraminiferal $\delta^{13}\text{C}$ values between the transect sites is large (up to $\sim 1.5\text{‰}$) during glacial periods MIC 6, 4, and 2; this suggests that different water masses bathed the north and south regions of this transect during each of these glacial periods (Fig. 5F; G).

The standard deviation (an indication of data spread) of the benthic foraminiferal $\delta^{13}\text{C}$ data shows higher values during MIC 6, 4, and the LGM ($>0.25\text{‰}$) relative to the spread in MIC 5e and 1; this shows that the southern portion of the transect is bathed by a different water mass than the northern portion. The difference between the northern and southern transect composite benthic foraminiferal $\delta^{13}\text{C}$ records are both also larger during these glacial periods, suggesting two distinct water masses (Fig. 5G). During MIC 6, 4 and the LGM, benthic

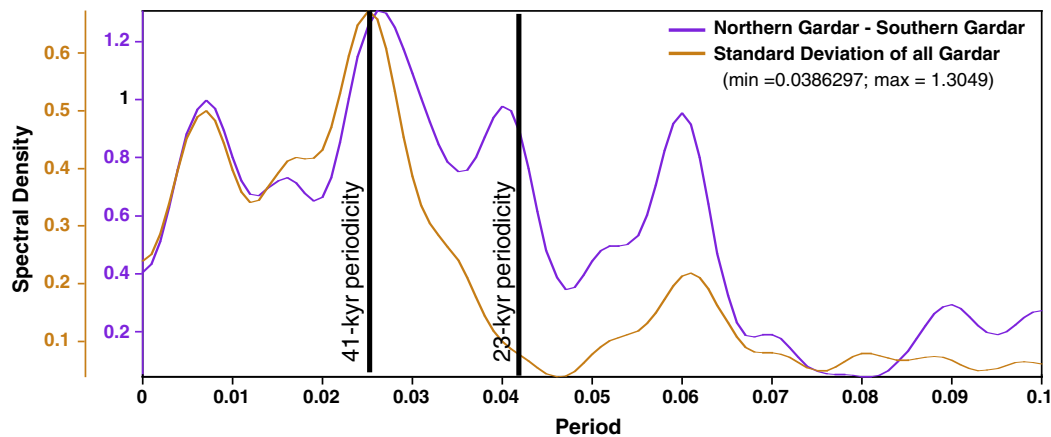


Fig. 6. Blackman–Tukey spectral analysis of the standard deviation benthic foraminiferal $\delta^{13}\text{C}$ values for the Gardar Drift transect from 0 to 200 ka (orange line) and of the difference between the smoothed Northern and Southern Gardar transects (purple line) determined using AnalySeries. Power can be seen in the obliquity (41 kyr) and precession (23 kyr) bands.

foraminiferal $\delta^{13}\text{C}$ values from southern Gardar Drift are more similar to values at DSDP 607 and ODP 1090 than the benthic foraminiferal $\delta^{13}\text{C}$ values at northernmost transect sites, indicating that SCW waters invaded the North Atlantic, reaching the southern flanks of Gardar Drift (Fig. 5F; G). Because of the location of this transect, the intrusion of SCW onto southern Gardar Drift is evidence for the shoaling of ISOW during glacial periods.

The warmer substages of MIC 5, 5e, 5c, and 5a are characterized by low (<0.5‰) benthic foraminiferal $\delta^{13}\text{C}$ variability on Gardar Drift (Fig. 5A; B). The standard deviation of the benthic foraminiferal $\delta^{13}\text{C}$ during MIC 5 is generally <0.25‰ (Fig. 5E). The difference between the northern and southern composite benthic foraminiferal $\delta^{13}\text{C}$ records is also lower during MIC 5e, 5c, 5a (Fig. 5F, G). The gradient is slightly larger during the cooler substages of MIC 5, MIC 5d, and 5b (~0.5‰; Fig. 5G). Increased difference between the northern and southern composite benthic foraminiferal $\delta^{13}\text{C}$ records and increased standard deviation of benthic foraminiferal $\delta^{13}\text{C}$ values during MIC 5d and 5b signify a greater range in benthic foraminiferal $\delta^{13}\text{C}$ values within the transect (Fig. 5G). This could suggest that ISOW was shallower during MIC 5d and 5b than during the other substages of MIC 5 (Fig. 5F, G). However, MIC 5d and 5b are characterized by ISOW that was only slightly shoaled.

Some higher-frequency variability is superimposed on the longer-term trends during MIC 4 and 3 in core 11JPC records of % CF, *G. bulloides* $\delta^{18}\text{O}$, *P. wuellerstorfi* $\delta^{13}\text{C}$, and % CaCO_3 (Fig. 2). Percent coarse fraction decreased from 70 to 60 ka and reached minimum values at ~58 ka, followed by a general increase from 58 to 35 ka (Fig. 2C). Percent carbonate and *P. wuellerstorfi* $\delta^{13}\text{C}$ records increased from 70 to 60 ka and reached maximum values at ~58 ka, followed by a general decrease in value from 58 to 35 ka (Fig. 2D, B). The period from 70 to 60 ka was characterized by a general decrease in the standard deviation of the benthic foraminiferal $\delta^{13}\text{C}$ values in the transect, followed by an increase in standard deviation from 58 to 35 ka, suggesting a shoaling of ISOW (Fig. 5G). *Globigerina bulloides* $\delta^{18}\text{O}$ values became increasingly variable during the period from 58 to 35 ka, suggesting changing surface water conditions that are attributed to increased freshwater inputs (Fig. 2A). Together, these records indicate an overarching change in circulation and climate whereby a general decrease in ice rafting and freshwater input leads to deepening of ISOW from 70 to 60 ka, and a general increase in ice rafting is linked to a shoaling ISOW from 58 to 35 ka (Figs. 2, 5).

Spectral analysis of the standard deviation of the benthic foraminiferal $\delta^{13}\text{C}$ values for the transect sites, which indicates the size of the gradient between northern and southern transect sites, reveals a strong precessional signal (Fig. 6). The precessional control on the north–south gradient indicates that the depth of ISOW penetration is paced by this orbital forcing (Fig. 6).

4. Discussion—Orbital scale variability in ISOW penetration depth

Variability in NCW formation is often linked to changes in insolation (Fig. 5B), known as Milankovich Cycles (Hays et al., 1976; Imbrie and Imbrie, 1980; Imbrie et al., 1993; Raymo, 1997; Raymo et al., 2004; Lisiecki and Raymo, 2005). Between 3 and 1 Ma, the 41-kyr obliquity cycles dominated benthic foraminiferal $\delta^{13}\text{C}$ records (Raymo et al., 1989; Raymo, 1997; Shackleton et al. 1990; Lisiecki and Raymo, 2005). Following the Mid-Pleistocene Climate Transition, the 100-kyr eccentricity cycle dominated ice volume trends through the late Pleistocene (Hays et al., 1976; Raymo et al., 2004; Lisiecki et al., 2008). Northern Component Water strength has been shown to follow these orbital-scale climate changes (e.g., Raymo et al., 2004). The depth of ISOW penetration also follows orbital-scale climate cycles with a strong 100-kyr periodicity (Figs. 5G, 6; Duplessy et al., 1988a; Kissel et al., 1997).

In addition to the longer eccentricity and obliquity cycles, the shorter ~23-kyr precession cycle is also visible in climate records (Fig. 6), most notably through the substages of MIC 5 (Raymo et al., 2004), as well as in the Mediterranean sapropels (Hilgen, 1991); however, precession is considered to be a weak driver of large-scale ice volume changes (Lisiecki et al., 2008). Precession-driven peaks in high-latitude northern hemisphere insolation can be seen at ~50 and ~60 ka (Fig. 5B; Laskar et al., 2004); however, previous studies of NCW strength do not show corresponding changes during MIC 3 (Raymo et al., 2004). Similarly, insolation peaks at ~150 and ~170 ka caused by the precessional forcing occur during MIC 6, which is generally presumed to be a prolonged glacial period of decreased NCW formation (Raymo et al., 2004).

Our benthic foraminiferal $\delta^{13}\text{C}$ records (Fig. 5D; F) indicate that ISOW penetrated to deeper water depths during interglacial periods, consistent with modern observations (Worthington, 1976) and other paleoceanographic reconstructions (Duplessy et al., 1988a,b; Kissel et al., 1997). During glacial periods, ISOW shoaled according to our records (Fig. 5F; G), consistent with proxy evidence for the intrusion of AABW into the northern North Atlantic (Boyle and Keigwin, 1987; Curry et al., 1988; Duplessy et al., 1988a,b; McManus et al., 1999; Marchitto et al., 2002; Curry and Oppo, 2005). This suggests that the general patterns of ISOW variability are driven by the 100-kyr eccentricity forcing. However, the variability in the benthic foraminiferal $\delta^{13}\text{C}$ values from the sites within the Gardar Drift transect also indicates that ISOW depth penetration varied in concert with precessional cycles (Figs. 5G; 6). These cycles are easily seen during the precession minima at ~185 and ~145 ka, during MIC 6, which are both associated with increased benthic foraminiferal $\delta^{13}\text{C}$ gradients from the standard deviation data, indicating shallower ISOW due to decreased insolation (Fig. 5G). These results are in opposition to those of Kuijpers et al. (1998), who suggested that ISOW formation was enhanced during

MIC 6. Additionally, the precessionally driven insolation minima at ~70 and ~25 ka and slight minima at ~45 ka have corresponding maxima in benthic foraminiferal $\delta^{13}\text{C}$ gradients (Figs. 5G; 6).

The mechanism that links precession cycles and ISOW strength must not be strictly temperature dependent since neither ice core (Alley, 2004) nor paleoceanographic temperature records show a pronounced precessional signal (Raymo et al., 2004; Lisiecki et al., 2008). However, we propose that high northern latitude summer insolation minima, driven mainly by precession cycles, led to increased low-elevation glaciers and sea-ice, which in turn provided the fresh meltwater necessary to impede convection in the Nordic Seas, and thus hindered the formation of ISOW. Additionally, the precessional forcing strongly affects low-latitude climate variations (McIntyre and Molino, 1996) and thus precessionally driven changes in the tropical carbon cycle could be driving the precessional variability seen in the Gardar Drift benthic foraminiferal $\delta^{13}\text{C}$ records.

A strong precessional control on ISOW strength (Fig. 6) is especially interesting considering that ISOW is a large contributor to NCW (Worthington, 1976), and precession is not considered to exert a strong control on NCW production strength (Raymo et al., 2004; Lisiecki et al., 2008). This apparent difference may be due to the fact that the Gardar Drift transect is in a confined, gateway location that is sensitive to even subtle changes in NCW. One possible explanation for the apparent disagreement between ISOW variations and NCW variations is that many NCW strength records do not have the temporal resolution to decipher precession-scale variability. Another possible explanation is that other NCW contributors compensate for decreased ISOW production during some precession minima; such orbital-scale variability has been seen in records of Denmark Straits Overflow Water (e.g., Fagel et al., 2002; Millo et al., 2006) and Labrador Sea Water (Hillaire-Marcel et al., 1994).

Our new benthic foraminiferal $\delta^{13}\text{C}$ data examine glacial–interglacial changes in the depth penetration of ISOW along the Gardar Drift, with interglacial ISOW penetrating more deeply than ISOW during glacial periods (Fig. 5). This may suggest a changing influence of ISOW to NADW during large climate transitions in the Late Pleistocene. Although $\delta^{13}\text{C}$ data are sometimes ambiguous, our carbon isotopic data provide an important constraint for a change in ISOW penetration depth since $\delta^{13}\text{C}$ is the only proxy that can currently provide the required data density to examine ISOW depth in 3 dimensions. Despite the limitations of $\delta^{13}\text{C}$, we have identified that ISOW was shallower during glacial intervals; since ISOW is a large contributor to NADW, this agrees with reconstructions that glacial NADW was shallower, weaker, or non-existent (e.g., Flower et al., 2000; Curry and Oppo, 2005; Lynch-Stieglitz et al., 2007; Thornalley et al., 2011a; Stern and Lisiecki, 2013). Indeed, there is a strong agreement between our Southern Gardar $\delta^{13}\text{C}$ record and the intermediate depth North Atlantic record from Lisiecki et al. (2008), suggesting that our records may have a wider importance to the North Atlantic (Fig. 5D). Our data also show SCW infringement on Southern Gardar Drift, which is in agreement with numerous reconstructions from the North Atlantic that demonstrate southern sourced water infringement using a variety of proxies from Pa/Th to Cd/Ca and neodymium isotopes (e.g., McManus et al., 1999; Marchitto et al., 2002; Alvarez Zarikian et al., 2009; Wilson et al., 2014). While our $\delta^{13}\text{C}$ data can only identify similar watermasses, and thus are not a direct link to ISOW volume or flow strength, sedimentological proxies in the region have suggested that glacial ISOW was weaker according to sediment magnetic properties (Kissel et al., 1999) or stronger according to grain-size and Sr/Nd isotopes. Both stronger and weaker ISOW strength can be reconciled with the shallower ISOW that we report.

5. Conclusions

Benthic foraminiferal $\delta^{13}\text{C}$ records from a Gardar Drift transect reveal that the depth of ISOW penetration varied on orbital timescales. Similar benthic foraminiferal $\delta^{13}\text{C}$ values were recorded along our

transect during MIC 5e and 1, indicating that ISOW was deeply penetrating during interglacial periods (Fig. 5D; Fig. 5F). During MIC 6, 4, and 2, ISOW shoaled significantly, allowing the intrusion of SCW into the southern region of Gardar Drift (Figs. 5G; 6). This relationship is consistent with previous studies linking NCW variation with the 100-kyr climate cycles of the late Pleistocene (e.g., Hays et al., 1976; Raymo et al., 1990, 2004). However, the Gardar Drift transect reveals a strong imprint of the precession component of insolation on ISOW production, particularly during intermediate climate states, such as MIC 3, and during the glacial states of MIC 6 and 4 (Figs. 5D; 6). The expression of precession in MIC 5 is strong in the climate signal (*cf.*, benthic foraminiferal $\delta^{18}\text{O}$ changes from MIC 5a to 5e) but muted in the $\delta^{13}\text{C}$ gradient on Gardar Drift. This suggests that during the substages of MIC 5, 1) ISOW production remained deeply penetrating, such that the mixing zone between NCW and SCW lay south of Gardar, and therefore Gardar Drift was insensitive to precession-driven changes, or 2) the smaller ice sheets in the northern hemisphere did not contribute substantial meltwater to the Norwegian Sea and therefore could not affect ISOW depth through either flux or density variations. On shorter timescales, high-frequency changes in ISOW penetration depth are also linked to freshwater inputs, likely due to Heinrich or Dansgaard–Oeschger Events.

Acknowledgements

We thank J. McManus, K. Miller, Y. Rosenthal, G. Mountain, and D. Thornalley for comments on earlier versions of this manuscript; K. Allen, L. Neitzke, S. Henderson, and R. Mortlock for helpful discussions; H. Evans and J. Channell for magnetostratigraphy; and J. Southon for AMS ^{14}C analytical assistance. The manuscript was significantly improved by comments from the editor and two anonymous reviewers. This research was supported by National Science Foundation grant OCE-0095219 to J.D. Wright. The data for this study will be permanently archived at <http://www.ncdc.noaa.gov/paleo/study/19339>.

References

- Alley, R.B., 2004. GISP2 ice core temperature and accumulation data. IGBP PAGES/World Data Center for Paleoclimatology Data Contribution Series. 13.
- Alvarez Zarikian, C.A., Stepanova, A.Y., Grutzner, Jens, 2009. Glacial-interglacial variability in deep sea ostracod assemblage composition at IODP Site U1314 in the subpolar North Atlantic. *Mar. Geol.* 258 (1–4), 69–87.
- Andrews, J.T., 2000. Icebergs and iceberg rafted detritus (IRD) in the North Atlantic: facts and assumptions. *Oceanography* 13 (3), 100–108.
- Bauch, H.A., Erlenkeuser, H., Spielhagen, R.F., Struck, U., Matthiessen, J., Thiede, J., Heinemeier, J., 2001. A multiproxy reconstruction of the evolution of deep and surface waters in the subarctic Nordic seas over the last 30,000 yr. *Quat. Sci. Rev.* 20, 659–678.
- Bianchi, G.G., McCave, N., 1999. Holocene periodicity in North Atlantic climate and deep-ocean flow south of Iceland. *Nature* 397, 515–517.
- Blackman, R.B., Tukey, J.W., 1958. *The Measurement of Power Spectra From the Point of View of Communication Engineering*. Dover Publications, New York (190 pp.).
- Bond, G.C., Lotti, R., 1995. Iceberg discharges into the North Atlantic on millennial time scales during the Last Glaciation. *Science* 267, 1005–1010.
- Boyle, E.A., Keigwin, L.D., 1987. North Atlantic thermohaline circulation during the past 20,000 years linked to high-latitude surface temperature. *Nature* 330, 35–40.
- Broecker, W.S., Denton, G.H., 1989. The role of ocean–atmosphere reorganizations in glacial cycles. *Geochim. Cosmochim. Acta* 53, 2465–2501.
- Broecker, W.S., Peteet, D.M., Rind, D., 1985. Does the ocean–atmosphere system have more than one stable mode of operation? *Nature* 315, 21–26.
- Channell, J.E.T., Hodell, D.A., Lehman, B., 1997. Relative geomagnetic paleointensity and $\delta^{18}\text{O}$ at ODP Site 983 (Gardar Drift, North Atlantic) since 350 ka. *Earth Planet. Sci. Lett.* 153, 103–118.
- Chapman, M.R., Shackleton, N.J., 1999. Global ice-volume fluctuations, North Atlantic ice-rafting events, and deep-ocean circulation changes between 130 and 70 ka. *Geology* 27 (9), 795–798.
- Charles, C.D., Fairbanks, R.G., 1992. Evidence from Southern Ocean sediments for the effect of North Atlantic deep-water flux on climate. *Nature* 355, 416–419.
- Coplen, T.B., Kendall, C., Hopple, J., 1983. Comparison of stable isotope reference samples. *Nature* 302, 236–238.
- Crocket, K.C., Vance, D., Gutjahr, M., Foster, G.L., Richards, D.A., 2011. Persistent Nordic deep-water overflow to the glacial North Atlantic. *Geology* 39, 515–518.
- Curry, W.B., Oppo, D.W., 2005. Glacial water mass geometry and the distribution of $\delta^{13}\text{C}$ and ΣCO_2 in the western Atlantic Ocean. *Paleoceanography* 20, 1–12.

- Curry, W.B., Duplessy, J.C., Labeyrie, L.D., Shackleton, N.J., 1988. Changes in the distribution of $\delta^{13}\text{C}$ of deep water ΣCO_2 between the Last Glaciation and the Holocene. *Paleoceanography* 3 (3), 317–341.
- Davies, T.A., Laughton, A.S., 1972. Sedimentary processes in the North Atlantic. In: Laughton, A.S., Berggren, W.A., et al. (Eds.), *Initial Reports of Deep Sea Drilling Project vol. 12*. U.S. Government Printing Office, Washington, D.C., pp. 905–934.
- Dickson, R.R., Gmitrowicz, E.M., Watson, A.J., 1990. Deep water renewal in the northern North Atlantic. *Nature* 344, 848–850.
- Dokken, T., Hald, M., 1996. Rapid climatic shifts during isotopes stages 2–4 in the Polar North Atlantic. *Geology* 24 (7), 599–602.
- Dokken, T.M., Nisancioglu, K.H., Li, C., Battisti, D.S., Kissel, C., 2013. Dansgaard–Oeschger cycles: interactions between ocean and sea ice intrinsic to the Nordic seas. *Paleoceanography* 28, 491–502. <http://dx.doi.org/10.1002/palo.20042>.
- Duplessy, J.C., Shackleton, N.J., Fairbanks, R.G., Labeyrie, L., Oppo, D.W., Kallel, N., 1988a. Deepwater source variations during the last climatic cycle and their impact on the global deep-water circulation. *Paleoceanography* 3 (3), 342–360.
- Duplessy, J.C., Labeyrie, L., Blanc, P.L., 1988b. Norwegian Sea Deep Water variations over the last climatic cycle: paleo-oceanographical implications. *Long Short Term Var. Clim.* 16, 86–116.
- Elmore, A.C., 2009. Late Pleistocene Changes in Northern Component Water. Ph.D. Thesis submitted to Rutgers University (299 pp.).
- Elmore, A.C., Wright, J.D., 2011. North Atlantic Deep Water and climate variability during the Younger Dryas cold period. *Geology* 39 (2), 107–110.
- Elmore, A.C., Wright, J.D., Southon, J., 2015. Continued meltwater influence on North Atlantic Deep Water instabilities during the early Holocene. *Mar. Geol.* 360, 17–24.
- Fagel, N., Innocent, C., Garipey, C., Hillaire-Marcel, C., 2002. Sources of Labrador Sea sediments since the last glacial maximum inferred from Nd–Pb isotopes. *Geochim. Cosmochim. Acta* 66 (14), 2569–2581.
- Fairbanks, R.G., Mortlock, R.A., Chiu, T.-C., Cao, L., Kaplan, A., Guilderson, T.P., Fairbanks, T.W., Bloom, A.L., Grootes, P.M., Nadeau, M.-J., 2005. Radiocarbon calibration curve spanning 0 to 50,000 years BP based on paired ^{230}Th , ^{234}U / ^{238}U and ^{14}C dates on pristine corals. *Quat. Sci. Rev.* 24, 1781–1796.
- Faugers, J.C., Stow, D.A.C., Imbert, P., Viana, A., 1999. Seismic features diagnostic of contourite drifts. *Mar. Geol.* 162, 1–38.
- Flower, B.P., Oppo, D.W., McManus, J.F., Venz, K.A., Hodell, D.A., Cullen, J.L., 2000. North Atlantic intermediate to deep water circulation and chemical stratification during the past 1 Myr. *Paleoceanography* 15, 388–403.
- Gebbie, G., 2014. How much did Glacial North Atlantic Water shoal? *Paleoceanography* 29 (3), 190–209.
- Hall, I.R., McCave, I.N., Chapman, M.R., Shackleton, N.J., 1998. Coherent deep flow variation in the Iceland and American basins during the last interglacial. *Earth Planet. Sci. Lett.* 164, 15–21.
- Hansen, B., Osterhus, S., 2000. North Atlantic–Nordic Seas exchange. *Prog. Oceanogr.* 45 (2), 109–208.
- Hátún, H., Sando, A.B., Drange, H., Bentsen, M., 2005. Seasonal to decadal temperature variations in the Faroe–Shetland inflow water. *Geophys. Monogr. Am. Geophys. Union* 158, 239.
- Hays, J.D., Imbrie, J., Shackleton, N.J., 1976. Variations in the Earth's orbit: pacemaker of the Ice Ages. *Science* 194 (4270), 1121–1134.
- Hilgen, F.J., 1991. Astronomical calibration of Gauss to Matuyama sapropels in the Mediterranean and implication for the Geomagnetic Polarity Time Scale. *Earth Planet. Sci. Lett.* 104, 226–244.
- Hillaire-Marcel, C., de Vernal, A., Lucotte, M., Mucci, A., 1994. The Labrador Sea during the late Quaternary. *Can. J. Earth Sci.* 31, 1–4.
- Hollister, C.D., Flood, R.D., McCave, I.N., 1978. Plastering and decorating in the North Atlantic. *Oceanus* 21 (1), 5–13.
- Imbrie, J., Imbrie, J.Z., 1980. Modeling the climatic response to orbital variations. *Science* 207 (4434), 943–953.
- Imbrie, J., Berger, A., Boyle, E.A., Clemens, S.C., Duffy, A., Howard, W.R., Kulka, G., Kitzbach, J., Martinon, D.G., McIntyre, A., Mix, A.C., Molino, B., Morley, J.J., Peterson, L.C., Pisias, N.G., Prell, W.L., Raymo, M.E., Shackleton, N.J., Toggweiler, J.R., 1993. On the structure and origin of major glaciation cycles 2. The 100,000-year cycle. *Paleoceanography* 8 (6), 699–736.
- Jansen, E., Raymo, M.E., Blum, P., et al., 1996. Site 983. *Proceedings of Ocean Drilling Program, Initial Reports* 162, pp. 139–167.
- Kissel, C., Laj, C., Lehman, B., Labeyrie, L., Bout-Roumazeilles, V., 1997. Changes in the strength of the Iceland–Scotland Overflow Water in the last 200,000 years: evidence from magnetic anisotropy analysis of core SU90-33. *Earth Planet. Sci. Lett.* 152, 25–36.
- Kissel, C., Laj, C., Labeyrie, L., Dokken, T., Voelker, A., Blamart, D., 1999. Rapid climatic variations during marine isotopic stage 3: magnetic analysis of sediments from Nordic Seas and North Atlantic. *Earth Planet. Sci. Lett.* 171, 489–502.
- Kleiven, H.F., Jansen, E., Curry, W.B., Hodell, D.A., Venz, K., 2003. Atlantic Ocean thermohaline circulation changes on orbital to sub-orbital timescales during the mid-Pleistocene. *Paleoceanography* 18 (1), 1–13.
- Kohl, A., Stammer, D., Cornuelle, B., 2007. Interannual to decadal changes in the ECCO Global Synthesis. *J. Phys. Oceanogr.* 27, 313–337.
- Kroopnick, P., 1985. The distribution of ^{13}C in the Atlantic Ocean. *Earth Planet. Sci. Lett.* 49, 469–484.
- Kroopnick, P., Weiss, R.F., Craig, H., 1972. Total CO_2 , ^{13}C , and dissolved oxygen- ^{18}O at GEOSECS II in the North Atlantic. *Earth Planet. Sci. Lett.* 16, 103–110.
- Kuijpers, A., Troelstra, S.R., Wisse, M., Nielsen, S.H., van Weering, T.C.E., 1998. Norwegian Sea overflow variability and NE Atlantic surface hydrography during the past 150,000 years. *Mar. Geol.* 152, 75–99.
- Laskar, J., Joutel, F., Boudin, F., 1993. Orbital, precessional, and insolation quantities for the Earth from -20 Myr to $+10$ Myr. *Astron. Astrophys.* 270, 522–533.
- Laskar, J., Robutel, P., Joutel, F., Gastineau, M., Correia, A.C.M., Levrard, B., 2004. A long-term numerical solution for the insolation quantities of the Earth. *Astron. Astrophys.* 428 (1), 261–285.
- Lisiecki, L.E., Raymo, M.E., 2005. A Pliocene–Pleistocene stack of 57 globally distributed benthic $\delta^{18}\text{O}$ records. *Paleoceanography* 20 (1003), 1–17.
- Lisiecki, L.E., Raymo, M.E., Curry, W.B., 2008. Atlantic overturning responses to Late Pleistocene climate forcings. *Nature* 456 (6), 85–88.
- Lynch-Stieglitz, J., Adkins, J.F., Curry, W.B., Dokken, T., Hall, I.R., Herguera, J.C., Hirschi, J.J.M., Ivanova, E.V., Kissell, C., Marchal, O., Marchitto, T.M., McCave, I.N., McManus, J.F., Mulitza, S., Ninnemann, U., Peeters, F., Yu, E.-F., Zahn, R., 2007. Atlantic meridional overturning circulation during the Last Glacial Maximum. *Science* 316, 66–69.
- Lynch-Stieglitz, J., Stocker, T.F., Broecker, W.S., Fairbanks, R.G., 1995. The influence of air-sea exchange on the isotopic composition of oceanic carbon: observations and modeling. *Glob. Biogeochem. Cycles* 9 (4), 653–665.
- Mackensen, A., Hubberten, H.-W., Bickert, T., Fischer, G., Futterer, D.K., 1993. The $\delta^{13}\text{C}$ in benthic foraminiferal tests of *Fonbotia wuellerstorfi* (Schwager) relative to the $\delta^{13}\text{C}$ of dissolved inorganic carbon in Southern Ocean deep water: Implications for glacial ocean circulation models. *Paleoceanography* 8 (5), 587–610.
- Marchitto, T.M., Oppo, D.W., Curry, W.B., 2002. Paired benthic foraminiferal Cd/Ca and Zn/Ca evidence for a greatly increased presence of Southern Ocean Water in the glacial North Atlantic. *Paleoceanography* 17 (3), 1–16.
- Mauritzen, C., 1996. Production of dense overflow waters feeding the North Atlantic across the Greenland–Scotland Ridge. Part 1: Evidence for a revised circulation scheme. *Deep-Sea Res. 1 Oceanogr. Res. Pap.* 4 (6), 769–806.
- McCave, I.N., Tucholke, B.E., 1986. Deep current-controlled sedimentation in the western North Atlantic. In: Vogt, P.R., Tucholke, B.E. (Eds.), *The Geology of North America, Vol. M, The Western North Atlantic Region*. Geological Society of America, Boulder, CO, pp. 451–468.
- McCave, I.N., Lonsdale, P.F., Hollister, C.D., Gardner, W.D., 1980. Sediment transport over the Hatton and Gardar Contourite Drifts. *J. Sediment. Petrol.* 50 (4), 1049–1062.
- McIntyre, A., Molino, B., 1996. Forcing of Atlantic equatorial and subpolar millennial cycles by precession. *Science* 274, 1867–1870.
- McIntyre, K., Ravelo, A.C., Delaney, M.L., 1999. North Atlantic Intermediate Waters in the late Pliocene to early Pleistocene. *Paleoceanography* 14, 324–335.
- McManus, J.F., Oppo, D.W., Cullen, J.L., 1999. A 0.5-million-year record of millennial-scale climate variability in the North Atlantic. *Science* 283, 971–975.
- Millo, C., Sarnthein, M., Voelker, A., Eriksenkeuser, H., 2006. Variability of the Denmark Strait Overflow during the Last Glacial Maximum. *Boreas* 1, 50–60.
- Moffa-Sanchez, P., Hall, I.R., Thornalley, D.J.R., Barker, S., Stewart, C., 2015. Changes in the strength of the Nordic Seas Overflows over the past 3000 years. *Quat. Sci. Rev.* 123, 134–143.
- Olsen, A., Ninnemann, U., 2010. Large $\delta^{13}\text{C}$ gradients in the preindustrial North Atlantic revealed. *Science* 330 (6004), 658–659.
- Oppo, D.W., Fairbanks, R.G., 1987. Variability in the deep and intermediate water circulation of the Atlantic Ocean during the past 25,000 years; Northern Hemisphere modulation of the Southern Ocean. *Earth Planet. Sci. Lett.* 86 (1), 1–15.
- Oppo, D.W., Horowitz, M., 2000. Glacial deep water geometry: South Atlantic benthic foraminiferal Cd/Ca and $\delta^{13}\text{C}$ evidence. *Paleoceanography* 15 (2), 147–160.
- Oppo, D.W., Lehman, S.J., 1995. Suborbital timescale variability of North Atlantic Deep Water during the past 200,000 years. *Paleoceanography* 10 (5), 901–910.
- Oppo, D.W., Raymo, M.E., Lohmann, G.P., Mix, A.C., Wright, J.D., Prell, W.L., 1995. A $\delta^{13}\text{C}$ record of Upper North Atlantic Deep Water during the past 2.6 million years. *Paleoceanography* 10 (3), 373–394.
- Oppo, D.W., Horowitz, M., Lehman, S.J., 1997. Marine core evidence for reduced deep water production during Termination II followed by a relatively stable substage 5e (Eemian). *Paleoceanography* 12, 51–63.
- Oppo, D.W., Keigwin, L.D., McManus, J.F., Cullen, J.L., 2001. Persistent suborbital climate variability in marine isotope stage 5 and Termination II. *Paleoceanography* 16 (3), 280.
- Ortiz, J.D., Mix, A., Harris, S., O'Connell, S., 1999. Diffuse spectral reflectance as a proxy for percent carbonate content in North Atlantic sediments. *Paleoceanography* 14, 171–186.
- Paillard, D., Labeyrie, L., Yiou, P., 1996. Macintosh program performs time-series analysis. *Eos. Trans. AGU* 77, 379.
- Praetorius, S.K., McManus, J.F., Oppo, D.W., Curry, W.B., 2008. Episodic reductions in bottom-water currents since the last ice age. *Nat. Geosci.* 1, 449–452.
- Prins, M.A., Troelstra, S.R., Kruk, R.W., van der Borg, K., de Jong, A.F.M., Weltje, G.J., 2001. The Late Quaternary sediment record of the Reykjanes Ridge, North Atlantic. *Radiocarbon* 43 (2B), 939–947.
- Prins, M.A., Bouwer, L.M., Beets, C.J., Troelstra, S.R., Weltje, G.J., 2002. Ocean circulation and iceberg discharge in the glacial North Atlantic: Inferences from unmixing of sediment size distribution. *Geology* 30 (6), 555–558.
- R Development Core Team, 2010. R: A language and environment for statistical computing. R Foundation for Statistical Computing, Vienna, Austria.
- Rasmussen, T.L., Thomsen, E., 2009. Ventilation changes in intermediate water on millennial time scales in the SE Nordic seas, 65–11 kyr BP. *Geophys. Res. Lett.* 36l, 1–5.
- Rasmussen, T.L., Thomsen, E., van Weering, T.C.E., Labeyrie, L., 1996a. Rapid changes in surface and deep water conditions at the Faeroe Margin during the last 58,000 years. *Paleoceanography* 11 (6), 757–771.
- Rasmussen, T.L., Thomsen, E., Labeyrie, L., van Weering, T.C.E., 1996b. Circulation changes in the Faeroe–Shetland Channel correlating with cold events during the Last Glacial Period (58–10 ka). *Geology* 24, 937–940.
- Rasmussen, T.L., Thomsen, E., Kuijpers, A., Wastegard, S., 2013. Late warming and early cooling of the sea surface in the Nordic seas during MIS 5e (Eemian Interglacial). *Quat. Sci. Rev.* 22 (8–9), 809–821.
- Raymo, M.E., 1997. The timing of major climate terminations. *Paleoceanography* 12, 577–585.

- Raymo, M.E., Ruddiman, W.F., Backman, J., Clement, B.M., Martinson, D.G., 1989. Late Pliocene variation in Northern Hemisphere ice sheets and North Atlantic deep water circulation. *Paleoceanography* 4, 413–446.
- Raymo, M.E., Ruddiman, W.F., Backman, J., Clement, B.M., Martinson, D.G., 1990. Evolution of Atlantic–Pacific $\delta^{13}\text{C}$ gradients over the last 2.5 my. *Earth Planet. Sci. Lett.* 97, 353–368.
- Raymo, M.E., Ganley, K., Carter, S., Oppo, D.W., McManus, J., 1998. Millennial-scale climate instability during the early Pleistocene epoch. *Nature* 392, 699–702.
- Raymo, M.E., Oppo, D.W., Flower, B.P., Hodell, D.A., McManus, J.F., Venz, K.A., Kleiven, K.F., McIntyre, K., 2004. Stability of North Atlantic water masses in face of pronounced climate variability during the Pleistocene. *Paleoceanography* 19, 1–13.
- Rind, D., Demenocal, P., Russel, G.L., Sheth, S., Collins, D., Schmidt, G.A., Teller, J., 2001. Effects of glacial meltwater in the GISS Coupled Atmosphere–Ocean Model: Part 1: North Atlantic Deep Water response. *J. Geophys. Res. Lett.* 106, 27335–27354.
- Roberts, N.L., Piotrowski, A.M., McManus, J.F., Keigwin, L.D., 2010. Synchronous deglacial overturning and water mass source changes. *Science* 327, 75–78.
- Ruddiman, W.F., 1977. Late Quaternary deposition of ice-rafted sand in the subpolar North Atlantic (lat 40 to 65N). *Geol. Soc. Am. Bull.* 88, 1813–1827.
- Ruddiman, W.F., McIntyre, A., Raymo, M.E., 1987. Paleoenvironmental results from North Atlantic sites 607 and 609. Initial Rep. Deep Sea Drill. Proj. 94, 855–878.
- Ruddiman, W.F., Raymo, M.E., Martinson, D.G., Clement, B.M., Backman, J., 1989. Mid-Pleistocene evolution of Northern Hemisphere climate. *Paleoceanography* 4, 353–412.
- Sarnthein, M., Winn, K., Jung, S.J.A., Duplessy, J.-C., Labeyrie, L., Erienkeuser, H., Ganssen, G., 1994. Changes in east Atlantic deepwater circulation over the last 30,000 years: eight time slice reconstructions. *Paleoceanography* 9 (2), 209–267.
- Sarnthein, M., Grootes, P.M., Kennett, J.P., Nadeau, M.-J., 2007. 14C reservoir ages show deglacial changes in ocean currents and carbon cycle. In: Schmittner, A., Chiang, J.C.H., Hemming, S.R. (Eds.), *Ocean Circulation: Mechanisms and Impacts—Past and Future Changes of Meridional Overturning*. American Geophysical Union, Washington, D.C. <http://dx.doi.org/10.1029/173GM13>.
- Schmitz, W.J., McCartney, M.S., 1993. On the North Atlantic Circulation. *Rev. Geophys.* 31 (1), 29–49.
- Shackleton, N.J., Berger, A., Peltier, W.R., 1990. An alternative astronomical calibration of the lower Pleistocene timescale based on ODP Site 677. *Trans. R. Soc. Edinb. Earth Sci.* 81 (4), 251–261.
- Stern, J.V., Lisiecki, L.E., 2013. North Atlantic circulation and reservoir age changes over the past 41,000 years. *Geophys. Res. Lett.* 40 (14), 3693–3697.
- Thornalley, D.J.R., McCave, I.N., Elderfield, H., 2010. Freshwater input and abrupt deglacial climate change in the North Atlantic. *Paleoceanography* 25 (1).
- Thornalley, D.J.R., Barker, S., Broecker, W.S., Elderfield, H., McCave, I.N., 2011a. The deglacial evolution of North Atlantic Deep Convection. *Science* 331 (6014), 202–205.
- Thornalley, D.J.R., McCave, I.N., Elderfield, H., 2011b. Tephra in deglacial ocean sediments south of Iceland: stratigraphy, geochemistry and oceanic reservoir ages. *J. Quat. Sci.* 26 (2), 190–198.
- Turrell, W.R., Slesser, G., Adams, R.D., Payne, R., Gillibrand, P.A., 1999. Decadal variability in the composition of Faroe Shetland Channel bottom water. *Deep Sea Res. Part I* 46, 1–25.
- Venz, K.A., Hodell, D.A., 2002. New evidence for changes in Plio-Pleistocene deep circulation from Southern Ocean ODP Leg 177 Site 1090. *Palaeogeogr. Palaeoclimatol. Palaeoecol.* 182, 197–220.
- Venz, K.A., Hodell, D.A., Stanton, C., Warnke, D.A., 1999. A 1.0 Myr record of Glacial North Atlantic Intermediate Water variability from ODP site 982 in the northeast Atlantic. *Paleoceanography* 14 (1), 42–52.
- Wilson, D.J., Crocket, K.C., van de Flierdt, T., Robinson, L., Adkins, J.F., 2014. Dynamic intermediate ocean circulation in the North Atlantic during Heinrich Stadial 1: a radiocarbon and neodymium isotope perspective. *Paleoceanography* 29 (11), 1072–1093.
- Winsor, K., Carlson, A.E., Klinkhammer, G.P., Stoner, J.S., Hatfield, R.G., 2012. Evolution of the northeast Labrador Sea during the last interglaciation. *Geochem. Geophys. Geosyst.* 13 (11), 1–17.
- Worthington, L.V., 1976. *On the North Atlantic Circulation*. Johns Hopkins University Press, Baltimore, MD.
- Wright, J.D., Miller, K.G., 1996. Control of North Atlantic Deep Water circulation by the Greenland–Scotland Ridge. *Paleoceanography* 11 (2), 157–170.
- Yu, J., Elderfield, H., Piotrowski, A.M., 2008. Seawater carbonate ion- $\delta^{13}\text{C}$ systematics and application to glacial-interglacial North Atlantic Ocean circulation. *Earth Planet. Sci. Lett.* 271 (1–4), 209–220.